

The design of conservative finite element discretisations for the vectorial modified KdV equation

Article

Accepted Version

Creative Commons: Attribution-Noncommercial-No Derivative Works 4.0

Jackaman, J., Papamikos, G. and Pryer, T. (2019) The design of conservative finite element discretisations for the vectorial modified KdV equation. *Applied Numerical Mathematics*, 137. pp. 230-251. ISSN 0168-9274 doi: <https://doi.org/10.1016/j.apnum.2018.10.006> Available at <https://centaur.reading.ac.uk/81475/>

It is advisable to refer to the publisher's version if you intend to cite from the work. See [Guidance on citing](#).

To link to this article DOI: <http://dx.doi.org/10.1016/j.apnum.2018.10.006>

Publisher: Elsevier

All outputs in CentAUR are protected by Intellectual Property Rights law, including copyright law. Copyright and IPR is retained by the creators or other copyright holders. Terms and conditions for use of this material are defined in the [End User Agreement](#).

www.reading.ac.uk/centaur

CentAUR

Central Archive at the University of Reading

Reading's research outputs online

1 **An exponential model of urban geometry for use in radiative**
2 **transfer applications**

3 **Robin J. Hogan**

4
5 the date of receipt and acceptance should be inserted later

6 **Abstract** In radiative transfer schemes for urban areas it is common to approximate
7 urban geometry by infinitely long streets of constant width, or other very idealized
8 forms. For solar and thermal-infrared radiative transfer applications, we argue that
9 horizontal urban geometry is described uniquely by the probability distribution of
10 wall-to-wall separation distances. The analysis of building layout from contrasting
11 neighbourhoods in London and Los Angeles reveals this function to be well fitted by
12 an exponential distribution. Compared to the infinite-street model, this exponential
13 model of urban geometry is found to lead to a significantly more accurate description
14 of the rates of exchange of radiation between the sky, the walls and the streets of an
15 urban canopy.

16 **Keywords** Radiative transfer · Street canyon · Urban Meteorology

17 **1 Introduction**

18 With the increasing urbanization of the world's population (United Nations, 2015)
19 and the ever higher resolution of weather and climate models, there is a need to
20 improve the fidelity with which urban areas are represented in such models. This is
21 a pre-requisite for better prediction of the urban-heat-island effect and its impact on
22 both city inhabitants at street level and the atmosphere downstream (e.g. Grimmond
23 et al., 2010). The complexity and variety of urban structure, with streets of different
24 widths, intersections, parking areas and parks, presents a challenge for modelling
25 both the exchange of solar and thermal-infrared radiation, and the turbulent transport
26 of heat, momentum and pollutants. Inevitably the geometry must be simplified in
27 order that processes can be represented efficiently, and the complexity needs to be

R. J. Hogan
European Centre for Medium Range Weather Forecasts, Shinfield Park, Reading, RG2 9AX, United King-
dom. E-mail: r.j.hogan@ecmwf.int.
Additional affiliation: Department of Meteorology, University of Reading, United Kingdom.

28 commensurate with the small number of parameters that are typically available to
29 describe variations in urban geometry within regional and global models.

30 In the case of urban radiation schemes, a common simplification is to consider
31 an infinitely long street of fixed width with random azimuthal orientation relative to
32 the sun (e.g. Masson, 2000; Harman et al., 2004; Li et al., 2016). In the horizontal
33 plane, the geometry of this ‘infinite-street model’ can be described by just two
34 parameters: the fraction of built-up area occupied by buildings, λ_p , and the street
35 width, W . These are accompanied by the building height, H , which is typically assumed
36 constant. From these parameters, several radiative exchange factors (called
37 shape factors by Harman et al., 2004) can be computed such as the fraction of direct
38 (i.e. unscattered) solar radiation that penetrates down to street level, and the fraction
39 of diffuse radiation emitted or scattered by the walls that then intercepts another wall.
40 Somewhat more sophisticated descriptions of horizontal urban geometry have been
41 proposed, such as a regular array of square-based blocks with intersections at regular
42 intervals (Kondo et al., 2005), but in the intercomparison of urban models by Grim-
43 mond et al. (2010), only six of the 33 models described horizontal urban geometry
44 by anything more sophisticated than an infinite-street canyon. A number of models
45 now incorporate radiative interaction with buildings of different height (e.g. Martilli
46 et al., 2002; Schubert et al., 2012) and street trees (Krayenhoff et al., 2014; Redon
47 et al., 2017), but they are still typically underpinned by the infinite-street assumption.
48 Clearly there is a need to test and if necessary improve this assumption.

49 In this paper an alternative ‘exponential model’ for characterizing horizontal ur-
50 ban geometry is proposed and evaluated. It uses the same number of parameters as
51 the infinite-street model, yet has the potential to describe the much more complex
52 geometry of real cities. Section 2 demonstrates that for the purposes of radiation, hor-
53 izontal building layout may be described uniquely by the probability distribution of
54 wall-to-wall separation distances, and it is shown how the radiative exchange factors
55 may be derived from this function. Section 3 describes how the infinite-street model
56 may be posed in terms of this probability distribution, and confirms that the resulting
57 formulas for the radiative exchange factors match those in the literature. Section 4
58 introduces the exponential model, and derives alternative formulas for these factors.
59 Then in Sect. 5, probability distributions are derived from real building distributions
60 in residential and commercial parts of London and Los Angeles, and used to evaluate
61 the accuracy of the infinite-street and exponential models in terms of how well they
62 predict the ‘true’ radiative exchange factors. It is important to stress that radiative
63 exchange factors provide a convenient way of evaluating the validity of the two as-
64 sumptions for radiative transfer, but do not themselves represent the important effects
65 of street trees, buildings of different heights, or absorption by air in the urban canopy.
66 In Sect. 6 we discuss how the exponential model could be incorporated into more
67 sophisticated schemes that do capture these effects.

68 **2 Urban geometry in terms of probability distributions**

69 We here consider how best to describe the horizontal distribution of buildings, so
70 for simplicity we assume that all buildings are the same height (H) with flat roofs

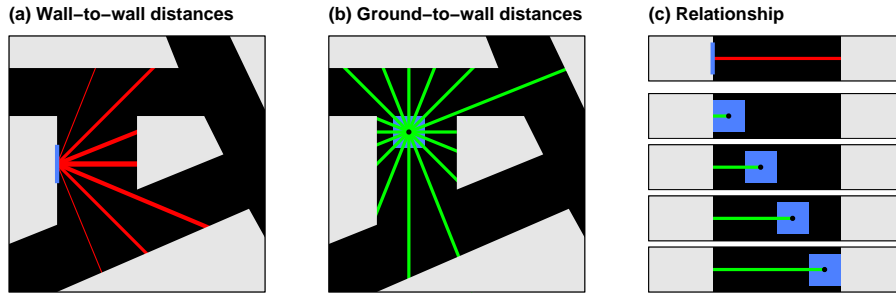


Fig. 1 Plan view of a small section of an urban canopy illustrating the definitions of the probability distributions p_{ww} and p_{gw} . (a) The red lines depict wall-to-wall distances x originating from a small vertical strip of wall (in blue); the probability distribution of x from all such strips is denoted $p_{ww}(x)$. The thickness of each line is proportional to the angle subtended by the strip in that particular direction. (b) The green lines depict the ground-to-wall distances x from a small facet of the ground (depicted by the blue square); the probability distribution of x from all such facets is denoted $p_{gw}(x)$. (c) Illustration of the property that a single wall-to-wall distance x' (the red line) is associated with ground-to-wall distances x in the range $0 < x < x'$ (shown by the four green lines), leading to the relationship between the two probability distributions given by (1). In each panel the buildings are shown in light grey and the ground in black.

71 and vertical walls. Consider diffuse radiation emitted or scattered from a thin verti-
 72 cal strip of wall in a particular azimuthal direction. Since radiation travels in straight
 73 lines, the probability of it being intercepted by another wall, rather than escaping to
 74 the atmosphere above or striking the ground, is a function of the distance between
 75 the two walls and their height. To determine the fraction of diffuse radiation emit-
 76 ted isotropically from all the walls in the neighbourhood that intercept another wall,
 77 we need to consider $p_{ww}(x)$, the probability distribution of wall-to-wall horizontal
 78 separation distances, x , considering all possible azimuth angles. Thus, a pedestrian
 79 walking away from a randomly selected point on a wall in a random direction has a
 80 probability $p_{ww}(x)dx$ of encountering another wall after walking a distance between
 81 x and $x + dx$. This is illustrated in Fig. 1a, where the variable thickness of the red lines
 82 highlights that the probability of radiation being emitted or scattered from the strip in
 83 a particular azimuthal direction ϕ varies as the cosine of the angle between ϕ and the
 84 wall normal.

85 For computing radiative exchanges between the ground (or street) and the walls,
 86 we need instead $p_{gw}(x)$, the probability distribution of ground-to-wall horizontal dis-
 87 tances within the urban canopy at all possible azimuth angles. In this case, a pedes-
 88 trian walking in a random direction from a randomly selected point at ground level
 89 has a probability $p_{gw}(x)dx$ of encountering a wall after walking a distance between x
 90 and $x + dx$, as illustrated in Fig. 1b.

91 There is a unique relationship between p_{ww} and p_{gw} , since as shown in Fig. 1c,
 92 any single wall-to-wall distance x' can be split into many ground-to-wall distances x ,
 93 where $x < x'$. Therefore, the probability density $p_{gw}(x)$ of a particular ground-to-wall

94 distance x is proportional to the probability of $x' > x$:

$$p'_{gw}(x) = \int_x^\infty p_{ww}(x') dx', \quad (1a)$$

$$p_{gw}(x) = p'_{gw}(x) / \int_0^\infty p'_{gw}(x) dx, \quad (1b)$$

95 where (1b) normalizes the ‘raw’ distribution p'_{gw} such that the normalized distribution
96 p_{gw} integrates to unity.

97 From these two probability distributions, and assuming a vacuum, we may com-
98 pute radiative exchange factors, F_{ij} , which denote the fraction of radiation originat-
99 ing from source i that illuminates destination j , where we assign the ground, wall
100 and ‘sky’ facets the subscripts g , w and s , respectively. We add an additional possible
101 source subscript ‘0’ denoting direct solar radiation from the sky facet, whereas all
102 other sources are diffuse. Some authors (e.g. Masson, 2000; Li et al., 2016) refer to
103 F_{ij} as ‘sky view factors’, but we avoid this term as it is more commonly used in the
104 literature to refer to the sky fraction viewed by an observer at a specific point on a
105 facet (e.g. Johnson and Watson, 1984), rather than integrated over all points on a facet
106 as signified by F_{ij} . All the equations for the F_{ij} exchange factors that follow involve
107 integration over one of the two probability distributions above, and may be applied
108 either analytically to parametric models for the probability distributions (as in Sects.
109 3 and 4), or numerically to probability distributions derived from real building layouts
110 (as in Sect. 5).

111 Consider first direct solar radiation, which travels horizontally a distance x_0 be-
112 tween the top and bottom of the urban canopy given by

$$x_0 = H \tan \theta_0, \quad (2)$$

113 where θ_0 is the solar zenith angle. This means that direct radiation entering the top of
114 the canopy at a particular point only penetrates to ground level if the nearest wall in
115 the azimuthal direction of the radiation is at least a distance x_0 away. Therefore, the
116 fraction F_{0g} of direct radiation just below canopy top that penetrates down to ground
117 level without being intercepted by a wall is

$$F_{0g} = \int_{x_0}^\infty p_{gw}(x) dx. \quad (3)$$

118 Any direct radiation just below canopy top that does not reach the ground must be
119 intercepted by a wall, so $F_{0w} = 1 - F_{0g}$.

120 The fraction of diffuse radiation emitted or scattered from ground level that is
121 intercepted by a wall is

$$F_{gw} = \int_0^\infty p_{gw}(x) f_{gw}(H/x) dx, \quad (4)$$

122 where $f_{gw}(H/x)$ is the fraction of diffuse radiation emitted from a small horizon-
123 tal area at ground level into the quadrant towards a wall of height H a distance x
124 away, which is intercepted by the wall. To derive an expression for f_{gw} , consider the
125 beam of radiation emitted from point A in Fig. 2a that intercepts the wall at point

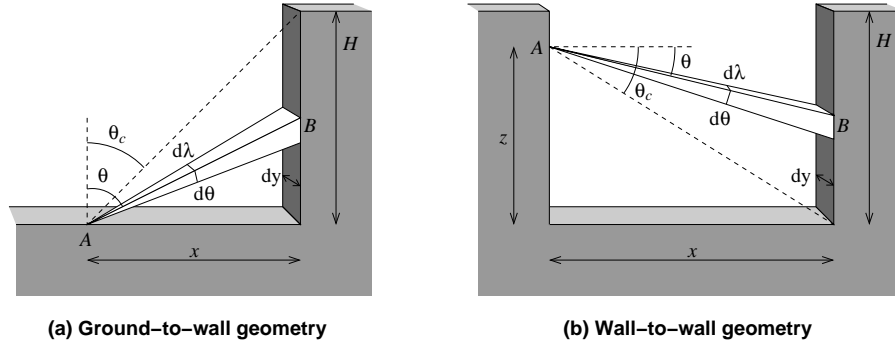


Fig. 2 Schematic of thin slices through an urban area illustrating the geometry used in Sect. 2 to compute the fraction of diffuse radiation emitted or scattered from (a) the ground and (b) a wall, which subsequently intercepts a wall. If the wall at B has an azimuthal orientation such that the light beam strikes it at an oblique azimuthal angle, then note that elemental length dy is the horizontal width of the beam, not the horizontal length of the wall at B that is illuminated by the beam (which could be larger).

126 B . If the emission is isotropic then the radiative power in this infinitesimally narrow beam is proportional to the solid angle $d\lambda d\theta$, multiplied by $\cos\theta$ to account
 127 for the dependence on θ of the angle subtended by the small horizontal area at A
 128 to an observer at B . From geometry we have $d\lambda = \sin\theta dy/x$, so the radiative power is
 129 proportional to $\sin\theta \cos\theta d\theta dy/x$. The fraction of radiative power emitted into the
 130 quadrant $0 < \theta < \pi/2$ that intercepts the wall is therefore given by
 131

$$f_{gw}(H/x) = \frac{\int_{\theta_c}^{\pi/2} \sin\theta \cos\theta d\theta}{\int_0^{\pi/2} \sin\theta \cos\theta d\theta}, \quad (5)$$

132 where the dy/x term is not a function of θ so cancels between numerator and denomi-
 133 nator. The critical zenith angle beyond which the beam starts to intersect the building
 134 is $\theta_c = \tan^{-1}(H/x)$, so (5) simplifies to

$$f_{gw}(H/x) = \frac{1}{1 + (x/H)^2}. \quad (6)$$

135 The fraction of diffuse radiation emanating from the ground that escapes to the
 136 sky is simply the fraction not intercepted by the walls, so we can write $F_{gs} = 1 - F_{gw}$,
 137 or equivalently

$$F_{gs} = \int_0^{\infty} p_{gw}(x) f_{gs}(H/x) dx, \quad (7)$$

138 where

$$f_{gs}(H/x) = 1 - f_{gw} = \frac{1}{1 + (H/x)^2}. \quad (8)$$

139 Moreover, the symmetry of the problem with respect to the sky and the ground im-
 140 plies that for diffuse radiation emanating from the sky we can write $F_{sg} = F_{gs}$ and
 141 $F_{sw} = F_{gw}$.

142 The fraction of diffuse radiation emitted or scattered from a wall that then en-
143 counters another wall is a function of the wall-to-wall probability distribution,

$$F_{ww} = \int_0^{\infty} p_{ww}(x) f_{ww}(H/x) dx, \quad (9)$$

144 where $f_{ww}(H/x)$ is the fraction of diffuse radiation emitted from a small width of
145 wall (but all heights up the wall) that intercepts another wall at distance x given that
146 the buildings are of height H . This calculation is more involved as we need to inte-
147 grate over all emission heights. We define $g_{ww}(z/x)$ as the fraction of diffuse radiation
148 emitted into the downward quadrant from a small area of wall at height z that inter-
149 cepts the other wall at distance x , rather than the ground. Consider the infinitesimally
150 narrow beam of radiation emitted from point A in Fig. 2b that arrives at point B . The
151 radiative power in the beam is again proportional to $\cos \theta d\lambda d\theta$, where θ is now the
152 angle relative a horizontal line emanating from the wall in the direction of B (not
153 necessarily the normal to the wall since the wall elements at A and B need not be
154 azimuthally parallel to each other). This time $d\lambda = \cos \theta dy/x$, so the radiative power
155 is proportional to $\cos^2 \theta d\theta dy/x$, leading to

$$g_{ww}(z/x) = \frac{\int_0^{\theta_c} \cos^2 \theta d\theta}{\int_0^{\pi/2} \cos^2 \theta d\theta} = \frac{2}{\pi} \left[\tan^{-1} \frac{z}{x} + \left(2 + \frac{z^2}{x^2} + \frac{x^2}{z^2} \right)^{-1/2} \right], \quad (10)$$

156 where the critical angle is $\theta_c = \tan^{-1}(z/x)$. Integrating g_{ww} over all heights up the
157 wall yields

$$f_{ww} = \frac{1}{H} \int_0^H g_{ww} dz = \frac{2}{\pi} \tan^{-1} \frac{H}{x}. \quad (11)$$

158 Note that here we have considered only radiation emitted into the downward quadrant
159 ($0 < \theta < \pi/2$ in Fig. 2b), but the symmetry of the problem means that the fraction
160 of diffuse radiation emitted from a wall into the equivalent upward quadrant that
161 intercepts another wall is the same, so (11) is valid for radiation emitted into either
162 quadrant.

163 In assessing different models for urban geometry, we shall use the equations in
164 this section to evaluate how well the models predict the exchange factors F_{0g} , F_{gs} and
165 F_{ww} . The other exchange factors are unique functions of these three; we have already
166 seen that $F_{0w} = 1 - F_{0g}$, $F_{gw} = 1 - F_{gs}$, $F_{sg} = F_{gs}$ and $F_{sw} = F_{gw}$. Furthermore, the
167 diffuse radiation emanating from a wall that does not hit another wall must be evenly
168 divided between the sky and the ground, so $F_{wg} = F_{ws} = (1 - F_{ww})/2$.

169 3 The infinite street canyon model

170 To demonstrate how the general approach in terms of probability distributions may be
171 applied to a specific geometry, we consider the case of infinitely long street canyons
172 of width W , a common assumption as discussed in Sect. 1. The wall-to-wall distance
173 in the horizontal plane is then given by

$$x = W / \cos \phi, \quad (12)$$

174 where ϕ is the azimuthal direction from the wall normal such that $\phi = 0$ is the direc-
 175 tion of shortest distance across the street, and $\phi = \pi/2$ is directed along the street. If
 176 the fraction of the urban area occupied by buildings is λ_p then the distance between
 177 adjacent streets in direction ϕ is $S = W / [(1 - \lambda_p) \cos \phi]$. The probability of wall-to-
 178 wall separation distances lying in the range x to $x + dx$ is then equal to the probability
 179 of azimuthal angles lying in the range ϕ to $\phi + d\phi$, i.e.

$$p_{ww}(x)dx = p(\phi)d\phi. \quad (13)$$

180 Each azimuthal street orientation is equally likely, implying that $p(\phi)$ should be con-
 181 stant, but from the definition of S we see that the distance between streets in direction
 182 ϕ is proportional to $1/\cos \phi$, implying that the probability density of streets in direc-
 183 tion ϕ is actually $p(\phi) = \cos \phi$. Differentiating (12) and substituting into (13) yields
 184 $p_{ww} = \cos^3 \phi / (W \sin \phi)$. Using (12) to express this in terms of W and x , and rec-
 185 ognizing that this expression is only valid for distances larger than the street width,
 186 yields

$$p_{ww}(x, W) = \begin{cases} 0 & : x \leq W, \\ \frac{W^2}{x^2} (x^2 - W^2)^{-1/2} & : x > W. \end{cases} \quad (14)$$

187 The probability distribution of ground-to-wall distances is found by applying (1) to
 188 (14), to obtain

$$p_{gw}(x, W) = \frac{2}{\pi W} \left(1 - \sqrt{1 - \frac{\min(W, x)^2}{x^2}} \right). \quad (15)$$

189 The radiative exchange factors may now be derived. Applying (3) to (15) we
 190 obtain

$$F_{0g} = \frac{2}{\pi} \left[\frac{Y - x_0}{W} + \tan^{-1} \frac{W}{Y} \right], \quad (16)$$

191 where $Y = \max(x_0^2 - W^2, 0)^{1/2}$. This is mathematically equivalent to Eq. 13 of Mas-
 192 son (2000). Similarly we apply (7) and (8) to (15), and (9) and (11) to (14), to obtain
 193 (after considerable manipulation)

$$F_{gs} = \sqrt{\frac{H^2}{W^2} + 1} - \frac{H}{W}; \quad (17)$$

$$F_{ww} = \sqrt{\frac{W^2}{H^2} + 1} - \frac{W}{H}, \quad (18)$$

194 which match the relations found previously (e.g. Sparrow and Cess, 1970; Noilhan,
 195 1981; Masson, 2000; Harman et al., 2004).

4 The exponential model

In this section an alternative model for horizontal urban geometry is proposed in which the two probability distributions are assumed to follow an exponential distribution,

$$p_{ww}(x) = p_{gw}(x) = \exp(-x/X)/X, \quad (19)$$

which satisfies the relationship between the two distributions given by (1). This distribution was assumed for the separation of trees in the forest radiative-transfer scheme of Hogan et al. (2018). The validity of the exponential model for urban areas is evaluated using real building layouts in the next section. As with the infinite-street model, only one parameter is used to characterize the distribution, in this case the ‘e-folding’ building separation X . Since X is also the mean value of the exponential distribution, it can be interpreted physically as the mean wall-to-wall distance considering all directions (i.e. the mean length of the red lines in Fig. 1a) or the mean ground-to-wall distance (i.e. the mean length of the green lines in Fig. 1b). However, when fitting an exponential distribution to the geometry of real cities, the method described in Sect. 5 should be used rather than simply setting X to the observed mean wall-to-wall separation distance.

The radiative exchange factors may again be derived by applying the integrals in Sect. 2. The penetration of direct radiation to ground level also has an exponential form,

$$F_{0g} = \exp(-x_0/X), \quad (20)$$

where x_0 is given by (2). This is essentially the Beer-Lambert law, and indicates that the penetration of direct radiation through an urban scene obeying the exponential model is the same as the penetration of direct radiation through a turbid medium with an extinction coefficient that does not vary with height.

The radiative exchange factors for diffuse radiation have a more complex form,

$$F_{gs} = 1 + \zeta \left[\cos \zeta \left(\text{Si} \zeta - \frac{\pi}{2} \right) - \sin \zeta \text{Ci} \zeta \right]; \quad (21)$$

$$F_{ww} = 1 + \frac{2}{\pi} \left[\cos \zeta \left(\text{Si} \zeta - \frac{\pi}{2} \right) - \sin \zeta \text{Ci} \zeta \right] = 1 + \frac{2}{\pi \zeta} (F_{gs} - 1), \quad (22)$$

where $\zeta = H/X$, $\text{Si}(\cdot)$ is the sine integral and $\text{Ci}(\cdot)$ is the cosine integral. In an operational model, these exchange factors could be implemented efficiently as one-dimensional look-up tables or Padé approximants.

Figure 3 compares the radiative exchange factors between the infinite-street model and the exponential model, as a function of the ratio of total wall area A_w to total ground area A_g . In the case of the infinite street, the ratio is

$$A_w/A_g = 2H/W, \quad (23)$$

since there are two walls for every street. For the exponential model, we apply energy conservation principles: if each surface of the urban area is at the same temperature (including the sky) and has an emissivity of unity then the energy emitted from a surface equals the energy received. For the walls this leads to

$$A_w B = 2A_g F_{gw} B + A_w F_{ww} B, \quad (24)$$

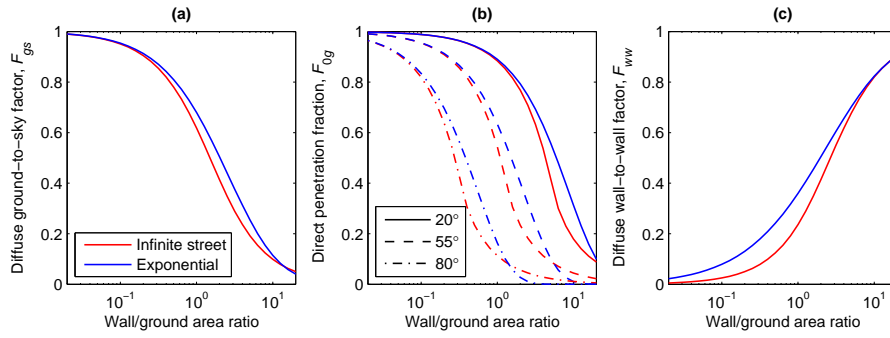


Fig. 3 Comparison of radiative exchange factors between the infinite-street model and the exponential model. The wall/ground area ratio, A_w/A_g , is defined in terms of the parameters of the two models by (23) and (25), and varies in the range 0.26–1.4 for the scenes analyzed in Sect. 5. Panel b shows F_{0g} for the three different solar zenith angles indicated in the legend.

230 where B is the power emitted per unit area (in W m^{-2}), the term on the left-hand
 231 side is the total power emitted from the walls, the first term on the right is the power
 232 received at the walls from the ground and sky (which is the same) and the second
 233 term on the right is the power received from other walls. Combining with (22), and
 234 noting again that $F_{gw} = 1 - F_{gs}$, we obtain

$$A_w/A_g = \pi H/X. \quad (25)$$

235 Equations 23 and 25 enable the two models to be plotted on the same axes in Fig. 3.
 236 These equations imply that the parameters W and X could be fitted to real cities from
 237 measurements of A_w/A_g , but in practice the wall area A_w is a somewhat ill-defined
 238 quantity in that it depends on the resolution of the measurements, and some buildings
 239 have fine-scale details that are not important for radiative exchange. Therefore we
 240 prefer the approach taken below, where W and X are fitted such that one of the radiative
 241 exchange factors is predicted exactly, and the validity of the model is assessed
 242 by how well the other factors are predicted.

243 5 Analysis of real cities

244 Here, the wall-to-wall and ground-to-wall probability distribution functions are computed
 245 for real cities, from which the radiative exchange factors are calculated numerically.
 246 This enables us to evaluate the different approximations to urban geometry described
 247 in Sects. 3 and 4. Building outlines and heights have been obtained for two cities,
 248 London and Los Angeles, and Fig. 4 depicts four $3 \text{ km} \times 3 \text{ km}$ scenes in which
 249 the buildings have been rendered on grid with a horizontal resolution of $\Delta x = 2 \text{ m}$.
 250 The scenes have been chosen to be very contrasting: the streets in Central London
 251 have an irregular layout and a range of different widths, the Residential London
 252 scene consists of a patchwork of rows of terraced housing, Downtown Los

253 Angeles consists of a grid layout with large buildings in each block, and the Residen-
 254 tial Los Angeles scene consists of a grid layout but with many small detached houses
 255 in each block. In the case of Central London, the location of the River Thames has
 256 been added manually using Google Maps imagery. The choice of 3×3 km domains
 257 is a compromise between the need for a scene to be large enough to sample streets of
 258 different orientation and to minimize sampling noise in the probability distributions,
 259 but small enough that the ‘character’ of the building layout is similar everywhere in
 260 a scene. The datasets do not contain information about the location of trees, which
 261 are known to be important for urban radiative transfer (Grimmond et al., 2010), but
 262 in Sect. 6 we discuss how our results could be incorporated into a more sophisticated
 263 urban radiation scheme that includes urban vegetation.

264 Before analyzing the building spacings, a question arises as to how to treat large
 265 open areas such as rivers and parks. Most global weather and climate models treat
 266 each gridbox of the surface by a number of tiles of different types, including open
 267 water, grassland and forest, in addition to urban. When green areas are small, such
 268 as gardens and small parks, their associated radiative and turbulent fluxes are sig-
 269 nificantly affected by nearby buildings and they are best treated as part of the urban
 270 tile. When they are large and most of their area is a long distance from the nearest
 271 building, it is more appropriate to treat them as a separate tile. However, there is no
 272 consensus on the size of the green space at which the transition should take place. We
 273 do not attempt to answer this question in this paper, but rather examine its effect on
 274 the probability distributions.

275 Contiguous regions of the domain that are at least 0.5 hectares in area and at
 276 least 20 m from the nearest building or river pixel have been identified automatically.
 277 Google Maps was then used to manually determine whether each such region is a
 278 parking area or plaza, a park, or a built-up surface not frequented by pedestrians
 279 (such as a railway or major highway). Parking areas and plazas are assigned to the
 280 same category as streets, while the other two are treated separately as shown in Fig. 4.
 281 The rationale of keeping major highways separate is that one of the main purposes of
 282 an urban model is to predict the conditions experienced by pedestrians at street level,
 283 but the impact of this decision is investigated below. The first three rows of Table 1
 284 list some basic properties of the four scenes.

285 Each gridded scene has been analyzed in four azimuthal directions, as illustrated
 286 in Fig. 5. Considering first the north–south and east–west directions in Figs. 5a and
 287 5b, the scene is analyzed in one-dimensional strips of width Δx , and in each strip the
 288 transitions from building-to-street and street-to-building are identified. From these
 289 the contiguous spans of the street category are identified, shown by the red lines.
 290 Note that in the first analysis any spans that include rivers, parks, railways or major
 291 highways are excluded, but in the second analysis towards the end of this section only
 292 those including rivers are excluded. Thus we may build up the probability distribution
 293 of wall-to-wall separation distances, p_{ww} , at the resolution of the grid (in this case
 294 2 m). A similar analysis of the diagonal strips (Figs. 5c and 5d) produces a probability
 295 distribution with a grid spacing $\sqrt{2}$ times larger. This is interpolated back on to the
 296 2-m grid and averaged with the first p_{ww} estimate, using a weighting that accounts
 297 for the fact that each diagonal strip is a factor of $\sqrt{2}$ times narrower. The probability
 298 distribution of ground-to-wall separation distances, p_{gw} , is computed by applying (1)

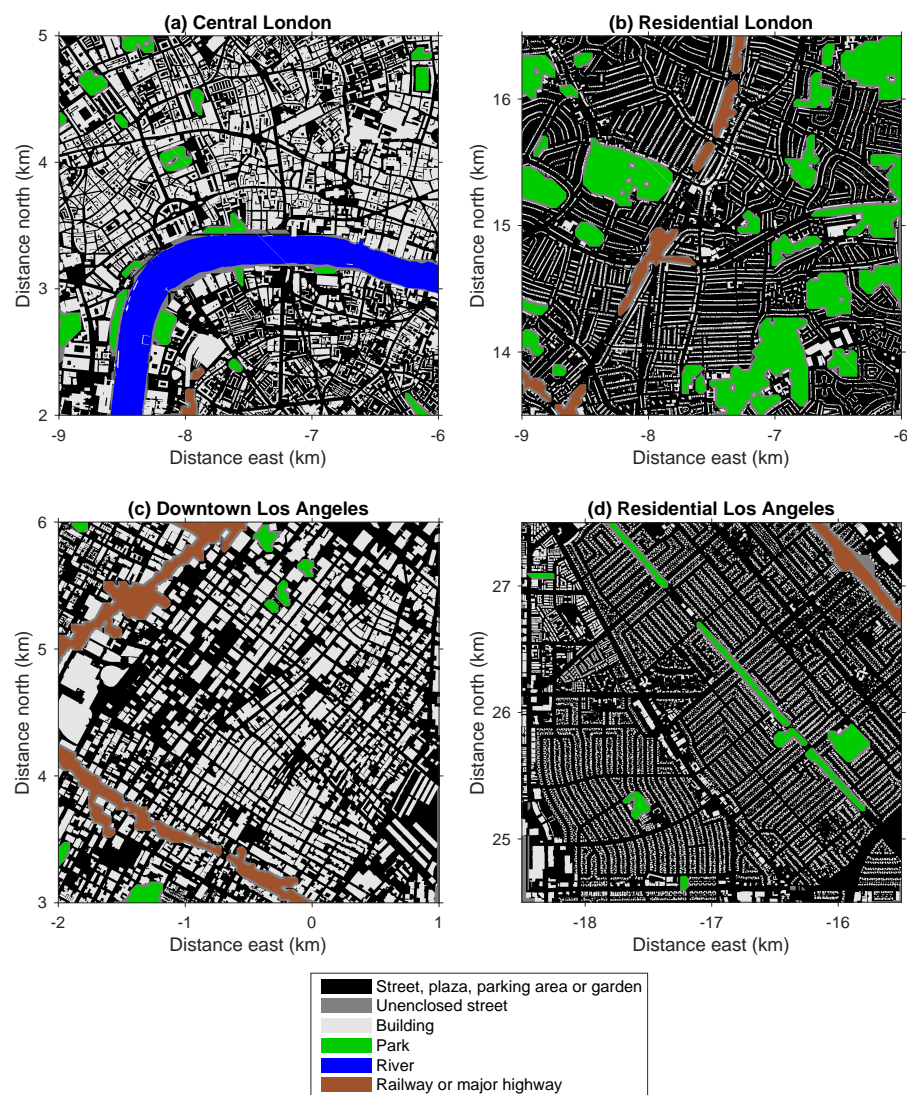


Fig. 4 Building layouts for four contrasting neighbourhoods of London and Los Angeles. The axes in the top two panels are indicated relative to a point 51.45°N , 0°E . The axes in the bottom two panels are indicated relative to a point 34°N , 118.25°W . Panel b shows the Palmers Green area of north London, while Panel d shows the Panorama City area of Los Angeles.

299 numerically to p_{ww} . A small fraction of the street pixels in the scene, particularly
 300 in the corners and at the borders of parks, are not sampled by this analysis in any
 301 of the four directions due to them not lying between two buildings in the directions
 302 considered; these are shown in dark grey in Fig. 4.

303 Care should be taken in applying the strip method of Fig. 5 to parts of several
 304 North American cities if all the streets are preferentially aligned along two of the strip

Table 1 Numerical properties of the four scenes depicted in Fig. 4. ‘Urban fraction’ is the fraction of the domain occupied by streets, plazas, parking areas, gardens or buildings, and ‘building fraction’ is the fraction of this urban area that is occupied by buildings. The street width (W) of the infinite-street model and the e-folding separation (X) of the exponential model have each been fitted to ensure that these models predict the ground-to-sky factor (F_{gs}) exactly. Therefore, the errors presented in the table are only for the predicted wall-to-wall factor (F_{ww}).

Property	Central London	Residential London	Downtown Los Angeles	Residential Los Angeles
Mean building height H (m)	17.0	6.6	19.7	4.8
Urban fraction	0.88	0.83	0.94	0.97
Building fraction λ_p	0.47	0.20	0.43	0.25
Diffuse ground-to-sky factor F_{gs}	0.60	0.84	0.66	0.88
Diffuse wall-to-wall factor F_{ww}	0.39	0.16	0.37	0.15
Fitted street width W (m)	32.0	38.8	46.4	36.0
Fitted e-folding separation X (m)	38.2	52.8	56.9	50.1
Error in F_{ww} from infinite-street model	−36%	−48%	−45%	−55%
Error in F_{ww} from exponential model	+10%	+27%	+3%	+18%

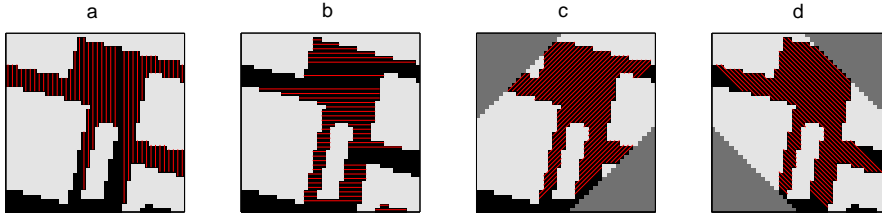


Fig. 5 Illustration of how the wall-to-wall probability distribution, $p_{ww}(x)$, is computed numerically from a digitized building layout, in this case considering an 80×80 -m subset of Fig. 4a at a resolution of 2 m. The scene is analyzed in four directions: (a) north–south, (b) east–west, (c) northeast–southwest and (d) northwest–southeast, and $p_{ww}(x)$ is constructed from the valid wall-to-wall distances x depicted by the red lines in each panel. The dark grey triangles in panels c and d are excluded from consideration since they are too small to contain the larger x values so could skew the distribution towards small x .

305 directions. One approach to mitigate potential biases would be to rotate the building
 306 polygon data by several different angles before discretizing to a grid and performing
 307 the strip analysis. There is some preference for northwest–southeast and northeast–
 308 southwest street orientation in the Residential Los Angeles scene (Fig. 4d), but we
 309 find below that the results for this scene are very similar to those from the Residential
 310 London scene (Fig. 4b), which has a much more random street orientation.

311 The black lines in Figs. 6a–6h depict the probability distributions derived from the
 312 four scenes. From these the various radiative exchange factors have been calculated
 313 numerically. The black lines in Fig. 6i–6k depict F_{0g} as a function of $\cos \theta_0$, while the
 314 diffuse factors F_{gs} and F_{ww} are shown in Table 1. Building height appears to be the
 315 dominant factor controlling radiative exchange, with the two downtown scenes hav-
 316 ing much lower penetrations of direct and diffuse radiation between sky and ground
 317 than the two residential areas.

318 We next investigate how well these distributions are fitted by the infinite-street and
 319 exponential models. The question arises of how best to fit the characteristic lengths

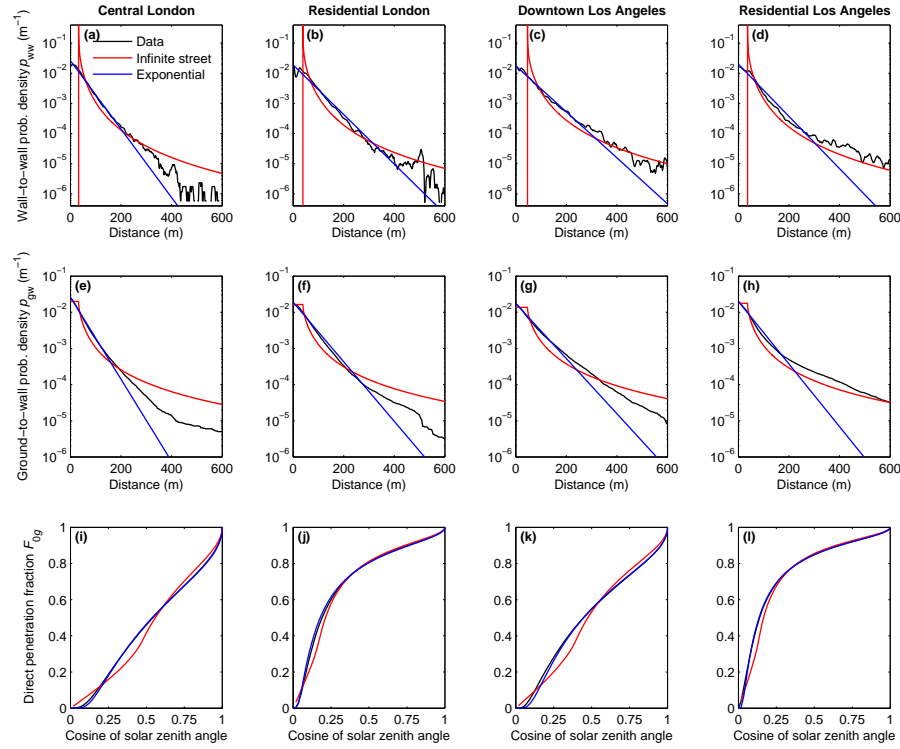


Fig. 6 (a–d) In black, the wall-to-wall probability distributions, p_{ww} , derived from the locations of the ‘street, plaza, parking area or garden’ category for the four scenes shown in Fig. 4. In red and blue, the fitted infinite-street and exponential models. (e–h) The corresponding ground-to-wall probability distributions, p_{gw} . (i–l) The corresponding direct penetration fraction F_{0g} as a function of the cosine of solar zenith angle.

320 for the two models, W and X . We have chosen to select these lengths such that the
 321 diffuse ground-to-sky exchange factor, F_{gs} , is predicted exactly. This is achieved by
 322 numerically inverting (17) and (21) to obtain the values of W and X from the observed
 323 values of F_{gs} and H ; the values obtained by this method are shown in Table 1. The
 324 associated analytical probability distributions for the two models (Eqs. 14, 15 and 19)
 325 are shown by the red and blue lines in Figs. 6a–6h. For all scenes, and for both p_{ww}
 326 and p_{gw} , the exponential distribution fits much better than the infinite-street model
 327 for building separations between 0 and at least 200 m. The infinite street is a particu-
 328 larly poor fit for $p_{ww}(x)$, predicting $p_{ww} = 0$ for $x < W$, a delta function at $x = W$,
 329 and an underestimation by around a factor of two at $x \approx 200$ m. For larger building
 330 separations there is more variability between scenes, but arguably the infinite-street
 331 model fits a little better.

332 The red and blue lines in Figs. 6i–6l depict the predicted direct sky-to-ground
 333 exchange factor, F_{0g} , revealing that the exponential model provides a better match to
 334 the values calculated from the real building distributions for all solar zenith angles.

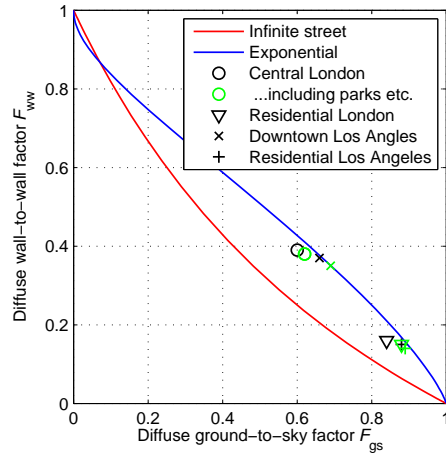


Fig. 7 Relationship between the diffuse wall-to-wall exchange factor F_{ww} and ground-to-sky exchange factor F_{gs} for the two analytic models (red and blue lines) and the four scenes depicted in Fig. 4 (black symbols). The green symbols depict the results from an alternative analysis of the four scenes in which parks, railways and major highways are added to the ‘street’ category.

335 This is because the probability distribution of building separations in the 0–200 m
 336 range, where the exponential model performs best, is more important for radiative
 337 exchange than larger building separations; indeed, only 1.0–3.9% of p_{ww} and 1.6–
 338 6.6% of p_{gw} is contained in building separations greater than 200 m.

339 In the case of diffuse exchange factors, the two models have already been fitted to
 340 ensure that F_{gs} is predicted exactly, but F_{ww} provides an independent point of evalua-
 341 tion. The lowest two rows of Table 1 show that the infinite-street model underpredicts
 342 F_{ww} by on average 46%, whereas the exponential model tends to overpredict F_{ww} but
 343 by only 15% on average. This is analyzed in more detail in Fig. 7, which depicts
 344 the unique relationships between F_{gs} and F_{ww} predicted by the two analytical models.
 345 The black symbols show the corresponding values for the four real scenes. The poorer
 346 performance of the infinite-street model is due to F_{ww} being particularly sensitive to
 347 $p_{ww}(x)$ for small x , where the two models are most different. Figure 3c also shows
 348 much lower F_{ww} for the infinite-street than the exponential model for wall/ground
 349 area ratios in the range found in these four scenes ($0.26 < A_w/A_g < 1.4$).

350 We now examine the impact of an alternative analysis of the four scenes, in which
 351 parks, railways and major highways are included in the ‘street’ category when deriv-
 352 ing wall-to-wall and ground-to-wall probability distributions. The results are shown
 353 in Fig. 8, revealing that the probability distributions show somewhat higher tails for
 354 the larger building separations, but the fitted exponential model still fits better for
 355 separations of less than 200 m, and also for the direct exchange factor shown in Figs.
 356 8i–8l. The green symbols in Fig. 7 show the F_{gs} and F_{ww} values for this alternative
 357 analysis, and again it is clear that the exponential model fits better.

358 If an urban radiation scheme using the exponential model were to be deployed
 359 in a weather or climate model then naturally the e-folding length X would first need

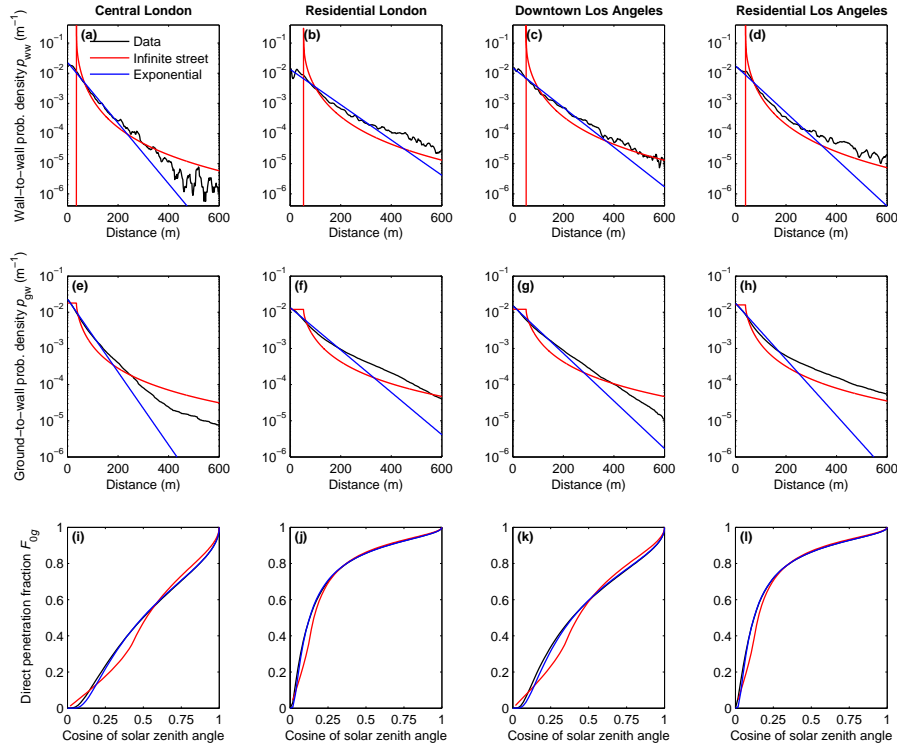


Fig. 8 As Fig. 6, but with parks, railways and major highways added to streets before performing the analysis.

360 to be estimated from the building layouts of a much larger number of cities. The
 361 strip method illustrated in Fig. 5 could of course be used to derive p_{ww} and p_{gw} , but
 362 the inversion of the rather complex relation (21) to find the value of X that predicts
 363 F_{gs} (and hence $F_{gw} = 1 - F_{gs}$) exactly could be regarded as cumbersome. A simpler
 364 approach is to instead find the value of X that predicts an approximate form of F_{gw} in
 365 which f_{gw} in (4) is replaced by an exponential of the form $f_{gw} \approx \exp(-x/Z)$, where
 366 Z is a length scale to be defined. This leads to the following formula for estimating X
 367 from an observed ground-to-wall probability distribution p_{gw} :

$$X \approx Z \left[\left(\int_0^\infty p_{gw} e^{-x/Z} dx \right)^{-1} - 1 \right]. \quad (26)$$

368 When used with a length scale of $Z = 1.5H$, the estimated values of X agree with
 369 those in Table 1 to within 1%. Mean building height H can be a somewhat ill-defined
 370 quantity in real cities, but we have found that using a fixed length scale of $Z = 10$ m
 371 also leads to acceptable results, with X estimates then agreeing with those in Table 1
 372 to within 1.2%.

373 6 Discussion and conclusions

374 In this paper it has been demonstrated that treating urban areas as streets of infinite
375 length and constant width, as done in many weather and climate models, leads to sig-
376 nificant errors in modelling the mean rates of exchange of solar and thermal-infrared
377 radiation between the sky, walls and ground. Analysis of the probability distributions
378 of wall-to-wall separation distances from real cities reveals that an exponential distri-
379 bution is a good fit, and leads to a significantly better prediction of radiative exchange
380 factors. Naturally, if this ‘exponential model’ of urban radiation were combined with
381 an existing treatment of turbulent fluxes to create a full urban exchange scheme, care
382 would need to be taken to ensure a consistent assumption about the areas of walls and
383 ground. The exponential model for urban geometry could also be useful for other ap-
384 plications sensitive to building layout, such as blockage of mobile telephone signals
385 (Bai et al., 2014).

386 While the radiative exchange formulas presented are a straightforward replace-
387 ment for those in ‘simple’ existing urban radiation schemes (such as that described
388 by Harman et al., 2004), an important question is how to incorporate the exponential
389 model into more sophisticated schemes (e.g. Schubert et al., 2012; Krayenhoff et al.,
390 2014; Redon et al., 2017) that represent vegetation and buildings of different height,
391 yet are still underpinned by the infinite-street assumption. One approach could be to
392 explore a useful property of the exponential model, which is that streams of radia-
393 tion with a particular zenith angle in an urban canopy are attenuated according to the
394 Beer-Lambert law, in the same way as light propagating through a turbid atmosphere.
395 Equation 20 demonstrates this for direct solar radiation, but it is applicable to the en-
396 tire radiation field if diffuse radiation is represented by a set of discrete zenith angles
397 (e.g. Stamnes et al., 1988), an approach that underpins almost all one-dimensional
398 multi-layer atmospheric radiative transfer schemes. This suggests that the infrastruc-
399 ture of such schemes could be adapted to the urban problem, enabling the prediction
400 of the vertical profile of radiation within an urban canopy containing buildings of
401 different heights, as well as the treatment of atmospheric absorption, emission and
402 scattering. Note that it is ubiquitous for current urban radiation schemes to treat the
403 space between buildings as a vacuum, but this is a dubious assumption in the thermal
404 infrared.

405 In terms of vegetation, Hogan et al. (2018) used ideas from one-dimensional at-
406 mospheric radiation schemes to develop an accurate multi-layer model for treating
407 radiation in forest canopies, embedded within which is the assumption that the hor-
408 izontal separation of obstacles (which could be trees or buildings) follows an ex-
409 ponential distribution. This would therefore be an appropriate starting point for a
410 more comprehensive urban radiation scheme that could accommodate street trees,
411 atmospheric effects and multiple building heights. Naturally a crucial step is to eval-
412 uate any new urban radiation scheme using calculations on real urban geometry
413 by explicit three-dimensional radiation models (e.g. Krayenhoff and Voogt, 2007;
414 Gastellu-Etchegorry, 2008; Lindberg et al., 2008).

415 **Acknowledgements** Robert Schoetter and Sue Grimmond are thanked for useful discussions. The build-
416 ing geometry for London was obtained from Emu Analytics, whose data combine building outlines from

417 Ordnance Survey Open Map with building height from lidar data collected in 2014 and 2015. Building
418 geometry data for Los Angeles were obtained from the Los Angeles County GIS Data Portal, with the
419 original data generated from aerial imagery. A number of the integrals were calculated using the online
420 symbolic integration tools at www.wolframalpha.com and www.integral-calculator.com.

421 References

- 422 Bai T, Vaze R, Heath RW (2014) Analysis of blockage effects on urban cellular networks. *IEEE Trans*
423 *Wireless Comm* 13:5070–5083
- 424 Gastellu-Etchegorry JP (2008) 3D modeling of satellite spectral images, radiation budget and energy
425 budget of urban landscapes. *Meteorol Atmos Phys* 102:187–207
- 426 Grimmond CS, Oke TR (1999) Aerodynamic properties of urban areas derived from analysis of surface
427 form. *J Appl Meteorol* 38:1262–1292
- 428 Grimmond CS, Blackett M, Best MJ, Barlow J, Baik J, Belcher SE, Bohnenstengel SI, Calmet I, Chen
429 F, Dandou A, Fortuniak K, Gouvea ML, Hamdi R, Hendry M, Kawai T, Kawamoto Y, Kondo H,
430 Krayenhoff ES, Lee S, Loridan T, Martilli A, Masson V, Miao S, Oleson K, Pigeon G, Porson A,
431 Ryu Y, Salamanca F, Shashua-Bar L, Steeneveld G, Tombrou M, Voogt J, Young D, Zhang N (2010)
432 The international urban energy balance models comparison project: first results from phase 1. *J Appl*
433 *Meteorol Climatol* 49:1268–1292
- 434 Harman IN, Best MJ, Belcher SE (2004) Radiative exchange in an urban street canyon. *Boundary-Layer*
435 *Meteorol* 110:301–316
- 436 Hogan RJ, Quaife T, Braghieri R (2018) Fast matrix treatment of 3-D radiative transfer in vegetation
437 canopies: SPARTACUS-Vegetation 1.1. *Geosci Model Dev* 11:339–350
- 438 Johnson GT, Watson ID (1984) The determination of view-factors in urban canyons. *J Clim Appl Mete-*
439 *orol* 23:329–335.
- 440 Krayenhoff ES, Voogt JA (2007) A microscale three-dimensional urban energy balance model for study-
441 ing surface temperatures. *Boundary-Layer Meteorol* 123:433–461
- 442 Krayenhoff ES, Christen A, Martilli A, Oke TR (2014) A multi-layer radiation model for urban neigh-
443 bourhoods with trees. *Boundary-Layer Meteorol* 151:139–178
- 444 Kondo H, Genchi Y, Kikegawa Y, Ohashi Y, Yoshikado H, Komiyama H (2005) Development of a multi-
445 layer urban canopy model for the analysis of energy consumption in a big city: structure of the urban
446 canopy model and its basic performance. *Boundary-Layer Meteorol* 116:395–421
- 447 Li D, Malyshev S, Shevliakova E (2016) Exploring historical and future urban climate in the Earth
448 System Modeling framework: 1. Model development and evaluation. *J Adv Model Earth Syst* 8:917–
449 935
- 450 Lindberg F, Holmer B, Thorsson S (2008) SOLWEIG 1.0 – Modelling spatial variations of 3D radiant
451 fluxes and mean radiant temperature in complex urban settings. *Int J Biometeorol* 52:697713
- 452 Martilli A, Clappier A, Rotach MW (2002) An urban surface exchange parameterisation for mesoscale
453 models. *Boundary-Layer Meteorol* 104:261–304
- 454 Masson V (2000) A physically-based scheme for the urban energy budget in atmospheric models.
455 *Boundary-Layer Meteorol* 94:357–397
- 456 Noilhan J (1981) A model for the net total radiation flux at the surfaces of a building. *Build Environ*
457 16:259–266
- 458 Redon EC, Lemonsu A, Masson V, Morille B, Musy M (2017) Implementation of street trees within the
459 solar radiative exchange parameterization of TEB in SURFEX v8.0. *Geosci Model Dev* 10:385–411
- 460 Schubert S, Grossman-Clarke S, Martilli, A (2012) A double-canyon radiation scheme for multi-layer
461 urban canopy models. *Boundary-Layer Meteorol* 145:439–468.
- 462 Sparrow EM, Cess RD (1970) *Radiation Heat Transfer*. Thermal Science Series, Brooks/Cole, Belmont
463 CA
- 464 Stammes K, Tsay SC, Wiscombe W, Jayaweera K (1988) Numerically stable algorithm for discrete-
465 ordinate-method radiative transfer in multiple scattering and emitting layered media. *Appl Opt*
466 27:2502–2509
- 467 United Nations (2015) *World Urbanization Prospects: The 2014 Revision*. U.N. Department of Economic
468 and Social Affairs, Population Division (ST/ESA/SER.A/366)